PHILOSOPHICAL TRANSACTIONS OF THE ROYAL SOCIETY A MATHEMATICAL, PHYSICAL & ENGINEERING SCIENCES

The effect of Mn-site doping on the magnetotransport properties of CMR manganites

A. Maignan, F. Damay, A. Barnab é, C. Martin, M. Hervieu and B. Raveau

Phil. Trans. R. Soc. Lond. A 1998 **356**, 1635-1659
doi: 10.1098/rsta.1998.0239

The Royal Society

The effect of Mn-site doping on the magnetotransport properties of CMR manganites

By A. Maignan, F. Damay, A. Barnabé, C. Martin, M. Hervieu and B. Raveau

Laboratoire CRISMAT, UMR 6508 associée au CNRS, ISMRA et Université de Caen 6, Boulevard du Maréchal Juin, 14050 CAEN Cedex, France

Doping of the Mn-site in $Ln_{1-y}A_yMn_{1-x}M_xO_3$ manganites has been extensively investigated. For the manganites exhibiting a Curie temperature (T_C) these substitutions depress T_C. However, the effect on T_C is doping-element dependent. It decreases from $dT_C/dx = -25\,K\,\%^{-1}$ for M = Fe down to $dT_C/dx \sim 0\,K\,\%^{-1}$ for M = Cr in the series $Sm_{0.56}Sr_{0.44}Mn_{1-x}M_xO_3$. The peculiar role of chromium doping is also shown in the case of the charge-ordered $Ln_{0.5}Ca_{0.5}MnO_3$-substituted manganites that are characterized by low average cationic size on the A-site and cationic size mismatch. For the latter, metal–insulator transitions together with CMR properties are induced by Cr and to a smaller extent by Co and Ni. The hindering of the charge-ordering establishment by these 'impurity effects' is also observed in the case of the two-dimensional manganites $La_{0.5}Sr_{1.5}MnO_4$ and $LaSr_2Mn_2O_7$. The highest efficiency of Cr among all doping elements may be ascribed to the similar t_{2g}^3 electronic configurations of Cr^{3+} and Mn^{4+} which allow a double-exchange between the Cr^{3+} and Mn^{3+} species.

Keywords: manganite; magnetoresistance; ferromagnetism; antiferromagnetism; Mn-site doping; insulator–metal

1. Introduction

A great deal of work has been devoted in the last few years to the $Ln_{1-y}A_yMnO_3$ manganites exhibiting colossal magnetoresistance (CMR) (von Helmolt *et al*. 1993; Chahara *et al*. 1993; Ju *et al*. 1994; Manoharan *et al*. 1994; Jin *et al*. 1994; Mahendiran *et al*. 1995; Mahesh *et al*. 1995*a*, *b*). The key parameters governing the Curie temperature, T_C, of these compounds and thus their CMR properties are the average size of the interpolated cation $\langle r_A \rangle$, the A-site cation size mismatch and the hole carrier density (Mahendiran *et al*. 1995; Mahesh *et al*. 1995*a*, *b*; Maignan *et al*. 1995*a*, *b*, 1996; Wang *et al*. 1995; Rodriguez-Martinez & Attfield 1996). Two classes of materials can be distinguished whose magnetotransport properties are roughly differentiated by the Mn^{4+} content, i.e. by y. For y values smaller than 0.5 ($Mn^{3+}/Mn^{4+} > 1$) a first class of materials is characterized by a transition from a ferromagnetic metallic (FMM) state below T_C to a paramagnetic insulating (PMI) state above T_C. The manganites $Ln_{0.7}A_{0.3}MnO_3$ and $Sm_{0.56}Sr_{0.44}MnO_3$ which belong to this family have been studied more closely (Mahendiran *et al*. 1995; Mahesh *et al*. 1995*a*, *b*; Maignan *et al*. 1995*a*, *b*, 1996; Wang *et al*. 1995; Rodriguez-Martinez & Attfield 1996; Damay

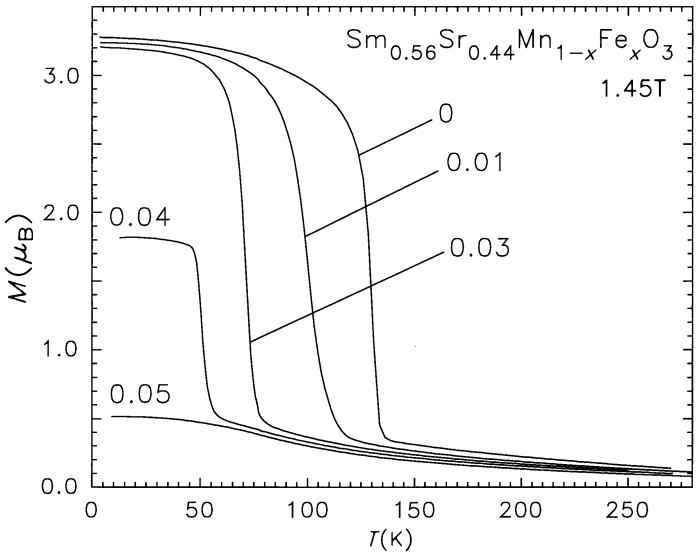

Figure 1. Temperature (T) dependence of the magnetization (M) for the iron-doped series $Sm_{0.56}Sr_{0.44}Mn_{1-x}Fe_xO_3$ (x values are labelled on the graph).

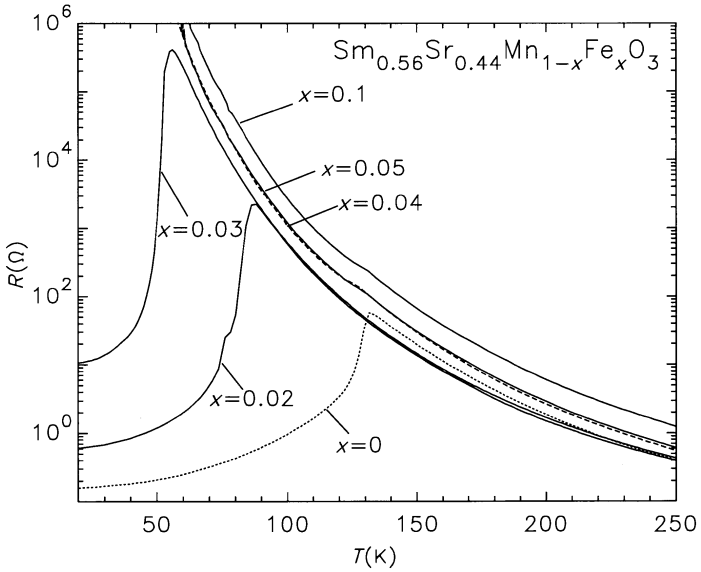

Figure 2. T dependence of the resistance (R) for $Sm_{0.56}Sr_{0.44}Mn_{1-x}Fe_xO_3$ samples.

et al. 1996*a*, *b*). The second class, which corresponds to $y = 0.5$ ($Mn^{3+}/Mn^{4+} = 1$) exhibits an additional transition from the FMM state to the antiferromagnetic insulating (AFMI) state below the Néel temperature, T_N, with $T_N < T_C$ as shown for the $Ln_{0.5}Sr_{0.5}$ compounds (Kuwahara *et al.* 1995; Tomioka *et al.* 1995; Kawano *et al.* 1997; Jirak *et al.* 1980, 1985; Wollan & Koehler 1955; Pollert *et al.* 1982). This AFMI state is favoured by the commensurate $Mn^{4+}/Mn^{3+} = 1$ ratio which for some –$Ln_{0.5}A_{0.5}$– compositions correspond to a charge-ordered (CO) state of the Mn^{3+}

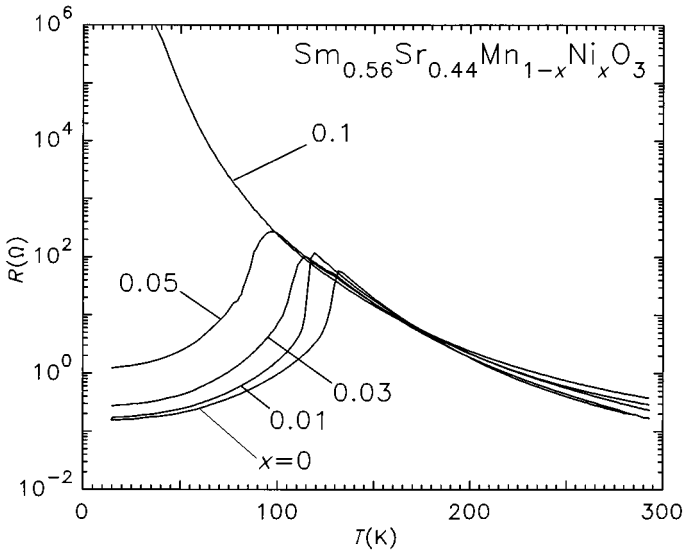

Figure 3. $R(T)$ curves for $Sm_{0.56}Sr_{0.44}Mn_{1-x}Ni_xO_3$ samples.

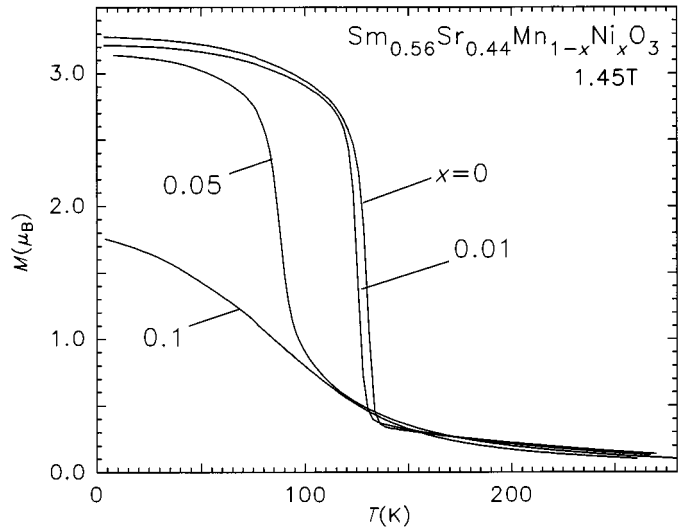

Figure 4. $M(T)$ curves for the series $Sm_{0.56}Sr_{0.44}Mn_{1-x}Ni_xO_3$.

and Mn^{4+} species below the charge-ordering temperature T_{CO} so that $T_{CO} = T_N$ (Jirak *et al*. 1980; Wollan & Koehler 1955).

The great analogy that exists between superconducting cuprates and CMR manganites suggests that the magnetotransport properties of the latter should be very sensitive to the doping of the manganese sites. In order to investigate the effect of Mn-site doping upon the magnetotransport properties in these manganites, we have substituted various elements for manganese. In the present paper we give an overview of our recent studies concerning the doping of Mn-sites in the two series $Sm_{0.56}Sr_{0.44}MnO_3$ and $Ln_{0.5}Ca_{0.5}MnO_3$ by various cations (M = Mg, Al, Fe, Ga, In, Ti, Sr, Cr, Co, Ni). In the first series, which exhibits a ferromagnetic-

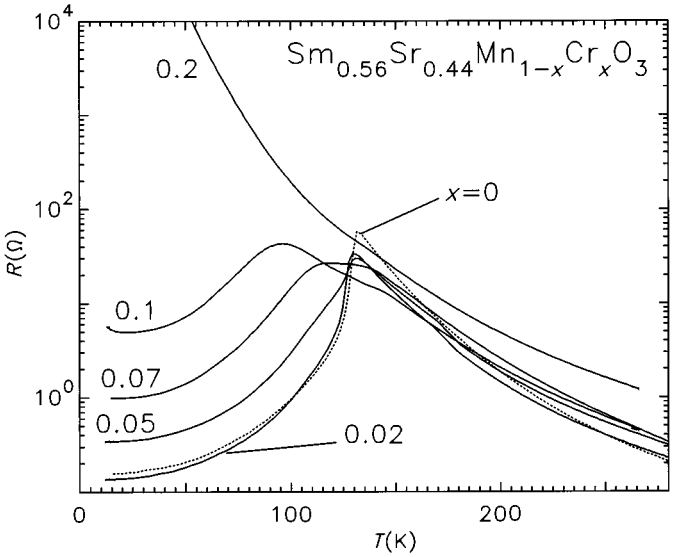

Figure 5. $R(T)$ curves for $Sm_{0.56}Sr_{0.44}Mn_{1-x}Cr_xO_3$ samples.

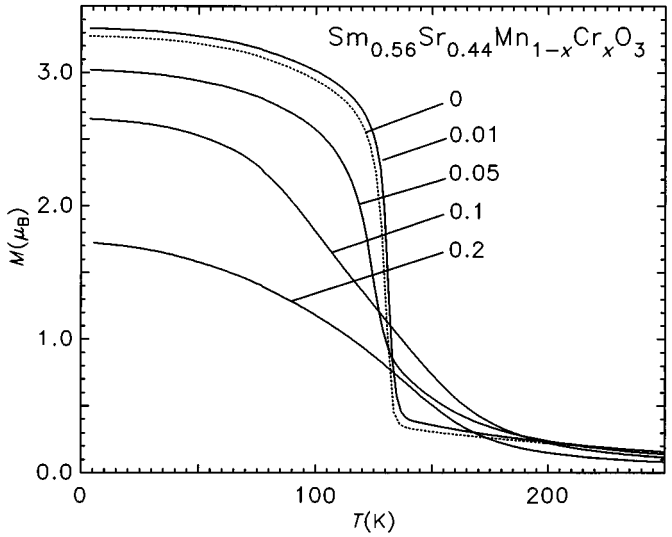

Figure 6. $M(T)$ curves for the $Sm_{0.56}Sr_{0.44}Mn_{1-x}Cr_xO_3$ series.

metallic–paramagnetic-insulating (FMM–PMI) transition, we demonstrate that with the exception of Cr, doping Mn-sites with foreign elements decreases T_C but generally increases the CMR effect in a spectacular manner. In the second series, we show that starting from insulating CO oxides, $Ln_{0.5}Ca_{0.5}MnO_3$, ferromagnetism and consequently CMR properties can be induced by just doping the Mn-sites. In the latter, the spectacular effect of doping with Cr, Co, Ni is described, showing that a MI transition is induced even in the absence of a magnetic field, so that the magnetic phase diagram based on the size and the mismatch of A-site cations is deeply modified by such a doping.

PHILOSOPHICAL TRANSACTIONS OF THE ROYAL SOCIETY A MATHEMATICAL, PHYSICAL & ENGINEERING SCIENCES

2. Substitutions in a charge delocalized manganite: $Sm_{0.56}Sr_{0.44}Mn_{1-x}M_xO_3$

The pure compound $Sm_{0.56}Sr_{0.44}MnO_3$ exhibits a transition from an FMM to a PMI state at $T_C = 130$ K (Damay *et al.* 1996*a*, *b*). This transition temperature is defined as the inflection point of the magnetization versus temperature curve registered in 1.45 T (figure 1, $x = 0$). On the resistance curve, the metal–insulator transition observed at $T_m = 130$ K as T increases corresponds to a resistivity maximum (figure 2, $x = 0$). The close values of T_C and T_m illustrate the strong interplay between the magnetic and electronic properties in this kind of material, called charge-delocalized (CD) materials because of the less resistive state observed below T_m (or T_C).

For this class of manganites, the Mn-site substitutions have been shown to decrease T_C (Damay *et al.* 1996*b*; Maignan *et al.* 1997*a*; Martin *et al.* 1996; Maignan & Raveau 1997). This was previously demonstrated for M = Mg^{2+}, Al^{3+}, Fe^{3+}, Ga^{3+}, In^{3+}, Ti^{4+} and Sn^{4+}, i.e. divalent, trivalent and tetravalent elements substituted for Mn in $Pr_{0.7}(Ca/Sr)_{0.3}MnO_3$ manganites (Maignan *et al.* 1997*a*; Martin *et al.* 1996; Maignan & Raveau 1997). Such a behaviour has also been observed for the compound $Sm_{0.56}Sr_{0.44}Mn_{1-x}M_xO_3$, whatever the doping element. A typical example is given for M = Fe in figures 1 and 2 for the T dependence of magnetization and resistance, respectively. From figure 2, one can see that T_m is strongly decreased from $T_m = 130$ K down to 85 K for only 2% Fe, and then to 55 K for 3% Fe. This dramatic decrease of T_m is strongly related to the corresponding drop of T_C shown on the $M(T)$ curves. Furthermore, for x values larger than 0.03, the saturation magnetization at 5 K tends to decrease so that for $x = 0.05$ the sample can no longer be described as a good ferromagnet. Thus it seems that Mn-site doping affects the ferromagnetic coupling energy. However, the effect on both T_m and T_C depends on the nature of the doping element. For instance, with M = Ni, the effect on the transitions is less severe (figures 3 and 4). On the resistance curves it is obvious that T_m is less sensitive to nickel substitutions (figure 3) than to iron substitutions (figure 2). Correspondingly, the saturation magnetization remains large (greater than $3\mu_B$) even for 5% of Ni (figure 4).

Finally, this kind of effect on the magnetotransport properties induced by Mn-site doping is evidenced for all doping elements except chromium. This cation, in its trivalent state, has the same electronic configuration t_{2g}^3 as Mn^{4+}. Moreover, the Mn^{3+}–O–Cr^{3+} superexchange interaction has been proposed to be ferromagnetic (Jonker 1956). The peculiar behaviour observed for M = Cr is illustrated on the $R(T)$ curves of figure 5. In contrast to M = Fe and Ni (figures 2 and 3) one can see that T_m values remain close to 130 K for values of x ranging from 0 to 0.05. For higher Cr contents, the $R(T)$ curves are characterized by double bumps, the flattest one appearing at about 130 K and the most pronounced one sitting below that temperature (see curves $x = 0.07$ and 0.10 in figure 5). The lack of effect on T_C for the lowest x values is corroborated by the $M(T)$ curves that emphasize the rather constant T_C values (taken as the inflection points on curves of figure 6). Moreover, the saturation magnetization values are by far the least sensitive for Cr doping ($x = 0.10$ curves for M = Fe, Co, Cr). For the highest x values, one can observe a broadening of the $M(T)$ curve transitions. This feature may be related to the different interaction energies between the Mn–Mn and Cr–Mn couples, the

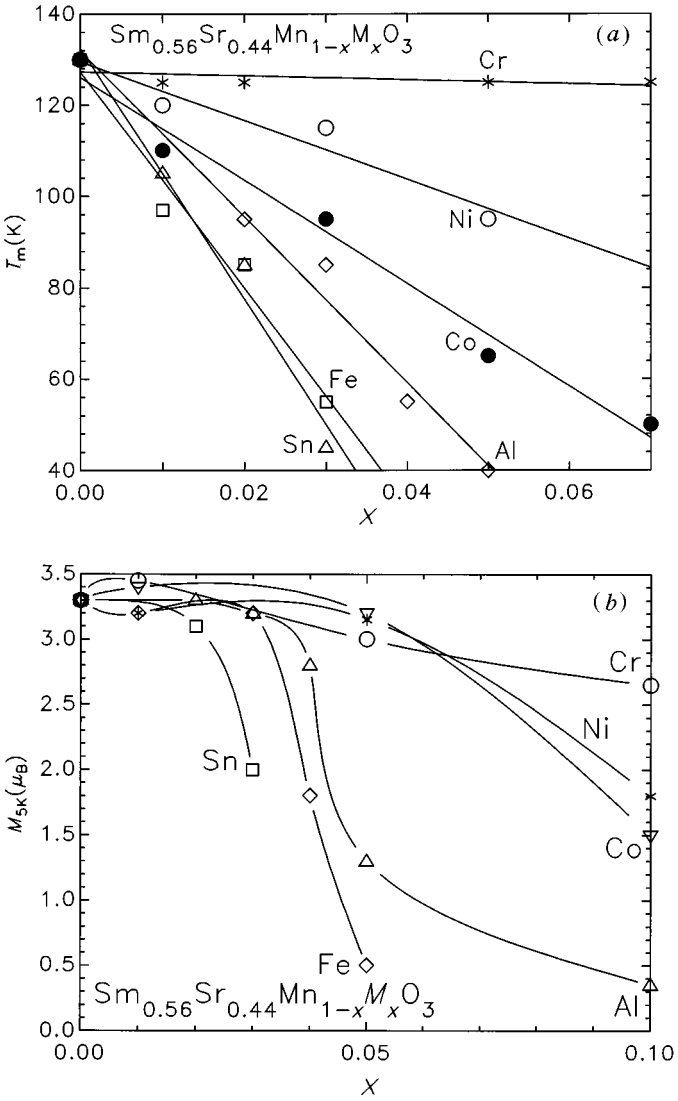

Figure 7. (*a*) T_{m} from the $R(T)$ curves versus x for the different $Sm_{0.56}Sr_{0.44}Mn_{1-x}M_xO_3$ series (lines are guides for the eye); (*b*) magnetization measured at $T = 5$ K ($M_{5\,\mathrm{K}}$) in 1.45 T after a zero field cooling versus x.

Mn^{3+}–Cr^{3+} one being appreciably smaller than that of Mn^{3+}–Mn^{4+} which governs the double-exchange ferromagnetism (Jonker 1956).

In order to summarize the results obtained for the different M-doping elements, the T_{m} values and saturation magnetization values ($M_{5\,\mathrm{K}}$) versus x in $Sm_{0.56}Sr_{0.44}Mn_{1-x}M_xO_3$ are shown in figure 7. The most efficient doping elements to decrease T_{C}, and consequently to suppress the ferromagnetism, are Fe and Sn ($\mathrm{d}T_{\mathrm{C}}/\mathrm{d}x = -25\ \mathrm{K}\ \%^{-1}$), this efficiency decreasing from Al ($-15\ \mathrm{K}\ \%^{-1}$) to Co ($-12\ \mathrm{K}\ \%^{-1}$) and finally to Ni ($-10\ \mathrm{K}\ \%^{-1}$) (figure 7*a*). This figure also emphasizes the peculiar effect induced by Cr since up to $x = 0.07$, T_{C} does not vary. Another way of comparing the abilities of

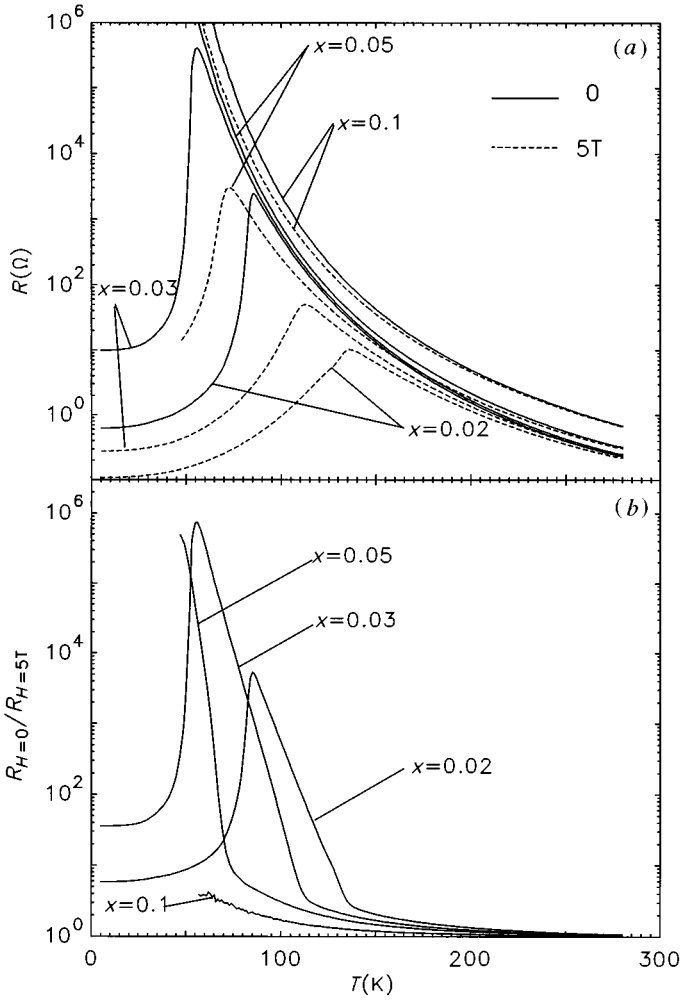

Figure 8. (top) $R(T)$ curves registered in 0 and 5 T for $Sm_{0.56}Sr_{0.44}Mn_{1-x}Fe_x$ samples; (bottom) corresponding T dependence of the resistance ratio $R_{H=0}/R_{H=5\,T}$.

ferromagnetism destruction is to consider the $M_{5\,K}(x)$ values (figure 7*b*). Only 3% Sn is sufficient to reduce $M_{5\,K}$ from $3.3\mu_B$ to $1.8\mu_B$, whereas 10% of Co and 20% of Cr (not shown) are needed to yield similar values.

These induced effects on the magnetotransport properties obviously lead to strong modifications of the CMR properties. For all doping elements, except chromium, this effect is illustrated by the behaviour of $Sm_{0.56}Sr_{0.44}Mn_{1-x}Fe_xO_3$ samples (figure 8). One can see on these curves, registered without applied magnetic field and in 5 T, that the substitution induces a T_m decrease which leads to a higher resistance ratio, RR ($RR = R_{H=0}/R_{H=5\,T}(T)$) in the vicinity of T_m. The RR increases from 30 for the pristine compound (not shown) to *ca.* 10^6 for $Sm_{0.56}Sr_{0.44}Mn_{0.97}Fe_{0.03}O_3$. For larger x values ($x > 0.03$), the $R(T)_{H=0}$ curves are characteristic of semiconducting samples, i.e. they do not exhibit peak behaviour. Nevertheless, the corresponding $R(T)_{H=5\,T}$ curves indicate a magnetic-field-induced MI transition (see $x = 0.05$

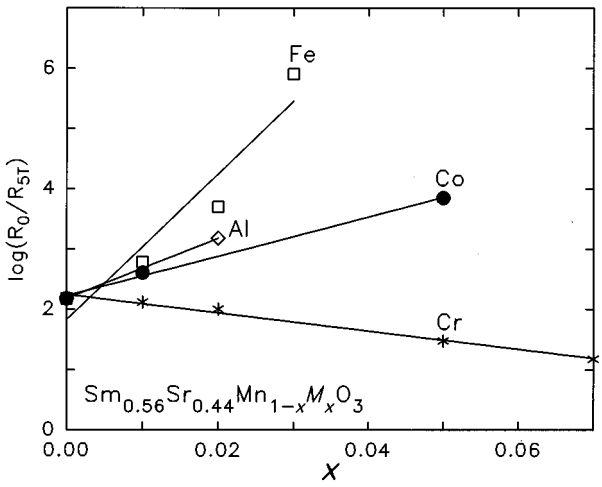

Figure 9. Dependence of the resistance ratio $R_0/R_{5\,\mathrm{T}}$ on x in the series $Sm_{0.56}Sr_{0.44}Mn_{1-x}M_xO_3$.

curve in figure 8). Moreover, the CMR effect tends to disappear as x increases; it becomes almost negligible for $x = 0.1$.

The huge CMR observed in these doped manganites is related to the fact that the $T > T_m$ parts of the $R(T)$ curves, registered without applied field, yield similar activation energies of *ca.* 120 meV although the R (280 K) values tend to increase with x. The doping weakens the ferromagnetic interactions, thus decreasing T_C and T_m. It results in an increase in the $R(T_{max})$ value as x increases so that the application of a magnetic field, which promotes the ferromagnetic metallic phase, leads to high RR values. In contrast, for the Cr-doped $Sm_{0.56}Sr_{0.44}Mn_{1-x}Cr_xO_3$ series, since T_{max} remains constant as x increases, at least for $x = 0.05$, the RR values are not strongly modified. Furthermore, as x increases, the magnetic field becomes less efficient in decreasing the resistance in the T_{max} vicinity so that RR tends to decrease slowly. The evolution of the maximum $R_{H=0}/R_{H=5\,\mathrm{T}}$ ratios versus x for the different doping elements (M = Fe, Al, Co, Cr) in the $Sm_{0.56}Sr_{0.44}Mn_{1-x}M_xO_3$ series are given in figure 9. Again, this graph emphasizes the different role played by chromium.

In conclusion, it appears thus that Mn-site doping provides a means of decreasing T_C in a controlled manner for these CD manganites. The observed results for the $Sm_{0.56}Sr_{0.44}Mn_{1-x}M_xO_3$ series can be extended to all CD manganites as shown in figure 10, where the $T_m(x)$ (or $T_C(x)$) values are reported for different iron-doped series of manganites. Clearly this effect is not strongly dependent on the average size of the A-site cations nor on the Mn^{4+} content since all the investigated series yield dT_C/dx slopes of *ca.* -25 K $\%^{-1}$ of Fe. Nevertheless, for M = Cr, the present results are totally different. One may speculate that this peculiar behaviour is linked to the isoelectronic configuration of both Mn^{4+} and Cr^{3+} species.

3. Substitutions on the Mn-site in charge-localized manganites

For this class of perovskites, the 'charge localized' (CL) expression refers to the existence of localized states for the transport properties occurring below T_N (corresponding to the appearance of the AFM state as T decreases). This kind of behaviour is

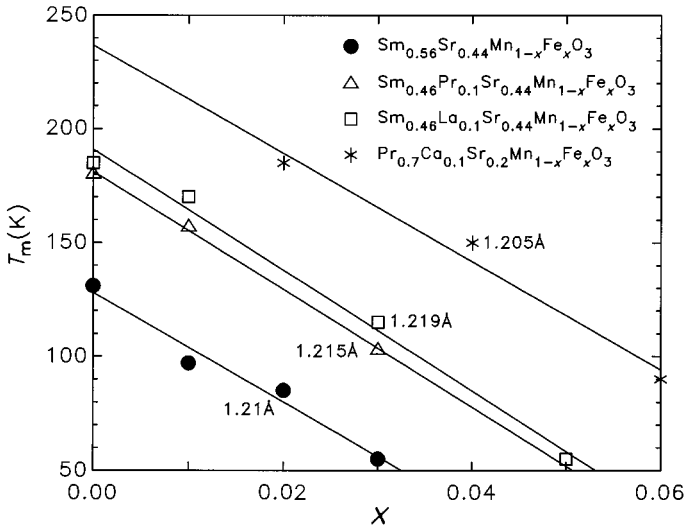

Figure 10. Dependence of T_m on x for different iron-substituted CD compounds in the series $Ln_{1-y}A_yMn_{1-x}Fe_xO_3$. The same slopes are observed whatever the series ($\langle r_A \rangle$ values are labelled on the graph).

usually encountered for the $Ln^{3+}_{0.5}A^{2+}_{0.5}MnO_3$ manganites where the $Mn^{4+}/Mn^{3+} = 1$ commensurate ratio favours different kinds of orderings for the Mn^{3+} and Mn^{4+} species in the lattice with various AFMI states. The prototype example of these CL compouds is the charge-ordered $Pr_{0.5}Ca_{0.5}MnO_3$ compound whose antiferromagnetic structure is of CE-type (Jirak *et al*. 1985). In the following, we will focus on the influence of both the average size of the A-site cations $\langle r_A \rangle$ and the A-site cationic size mismatch measured from the variance σ^2 ($\sigma^2 = \sum y_i r_i^2 - \langle r_A \rangle^2$, where r_i is the radius of the A-site cation and y_i is the fractional occupancy) on the magnetic properties of the $Ln_{0.5}A_{0.5}MnO_3$ compounds. We will then concentrate on the results of Mn-site substitutions obtained for the $Ln_{0.5}Ca_{0.5}MnO_3$ charge-ordered manganites, especially those which are characterized by small $\langle r_A \rangle$ and σ^2 values.

(*a*) $\langle r_A \rangle$ *and* σ^2*: key chemical parameters governing the properties of the* $Ln_{0.5}A_{0.5}MnO_3$ *compounds*

For the CD manganites such as $Ln_{0.7}A_{0.3}MnO_3$, it was shown early on that T_C (or T_m) is governed only by $\langle r_A \rangle$ (Mahendiran *et al*. 1995; Mahesh *et al*. 1995*a*, *b*; Maignan *et al*. 1995*a*, *b*, 1996; Wang *et al*. 1995). It was experimentally observed that T_C decreases as $\langle r_A \rangle$ decreases. Since then, Rodriguez-Martinez & Attfield (1996) have clearly demonstrated that, at a constant $\langle r_A \rangle$, T_C decreases as σ^2 increases. Clearly, both σ^2 and $\langle r_A \rangle$ have thus to be considered in order to predict the magnetotransport properties of these CD manganites.

This is also true if one wants to compare the $\langle r_A \rangle$ dependence of the magnetic properties of CL manganites. This study has been undertaken (Wolfman *et al*. 1996*a*, *b*) by varying x in the two series $Pr_{0.5}Sr_{0.5-x}Ca_xMnO_3$ and $Pr_{0.5-x}Y_xSr_{0.5}MnO_3$ where $\langle r_A \rangle$ decreases as x increases. The undoped $Pr_{0.5}Sr_{0.5}MnO_3$ compound exhibits two types of transitions (figure 11, curve $x = 0$). As T decreases from room temperature, the sample evolves from a PMI state for $T > T_C$ to an FMM state for $T < T_C$

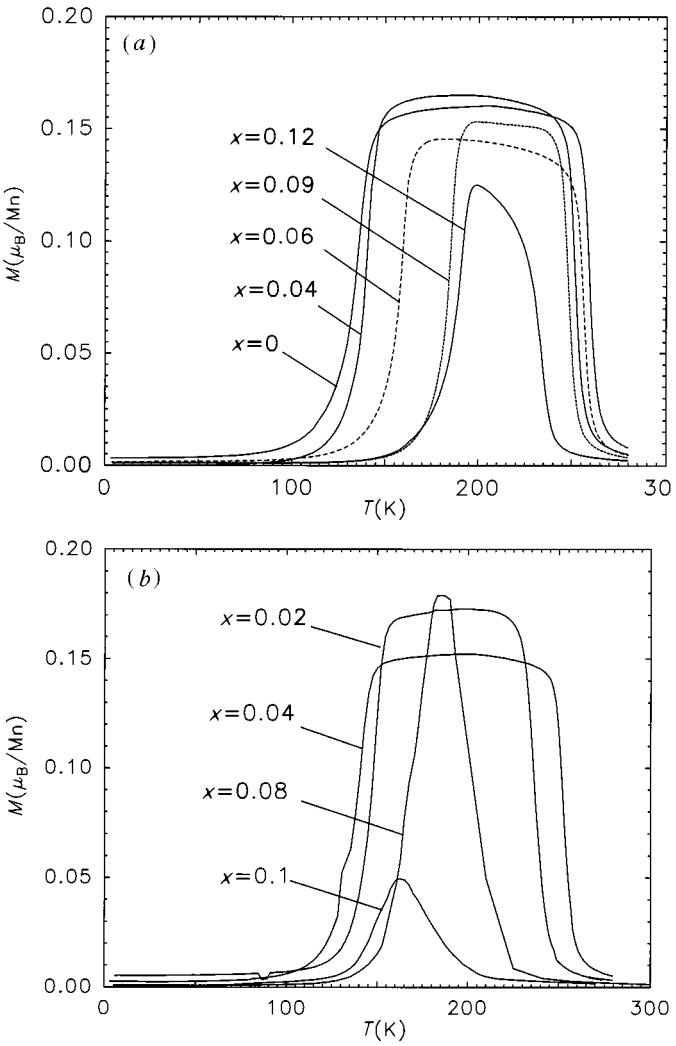

Figure 11. $M(T)$ curves (10^{-2} T) for the series (a) $Pr_{0.5}Sr_{0.5-x}Ca_xMnO_3$ and (b) $Pr_{0.5-x}Y_xSr_{0.5}MnO_3$.

and then switches to an AFMI state below T_N with $T_N < T_C$ (see curve $x = 0$ in figure 11a). Both Y and Ca substitutions lead to the same kind of evolution: T_C decreases whereas T_N increases as x increases (figure 11a, b). However, if one plots T_C and T_N versus $\langle r_A \rangle$ different curves are obtained. On the one hand T_N increases from 150 to 190 K as $\langle r_A \rangle$ decreases for the Ca series whereas T_N remains at a constant value of *ca.* 150 K for the Y series. On the other hand, T_C decreases faster with $\langle r_A \rangle$ for the Y series compared to the Ca series. The $T_C(\langle r_A \rangle)$ and $T_N(\langle r_A \rangle)$ results obtained for six different $(Ln,Ln')_{0.5}(A,A')_{0.5}MnO_3$ series (Damay *et al.* 1997a, b) are compiled in figure 12. It is clearly shown that $T_C(\langle r_A \rangle)$ curves of the $Ln_{0.5}(Sr,Ca)_{0.5}MnO_3$ series are smoother than the corresponding curves of the $(Ln,Ln')_{0.5}Sr_{0.5}MnO_3$ series. Consequently, for the (Sr,Ca) series T_N reaches the highest values. These apparent discrepancies between the different series can be easily explained by considering

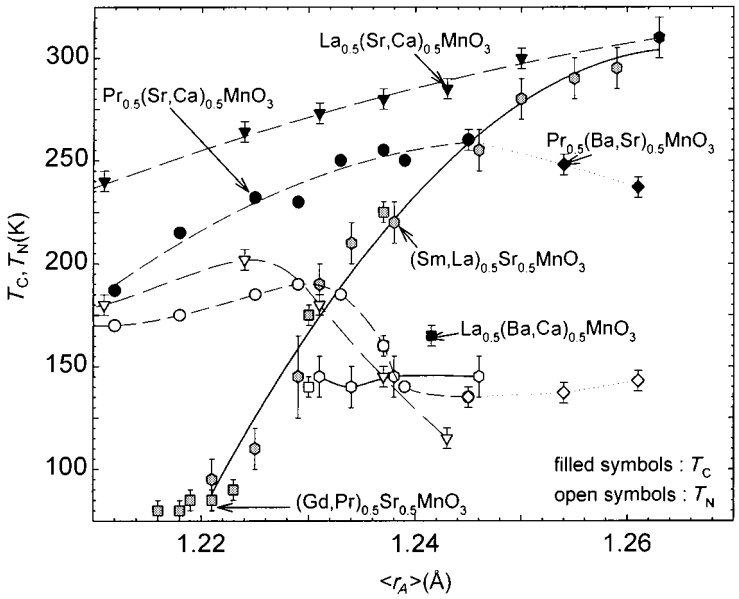

Figure 12. Curie temperatures (T_C) and Néel temperatures (T_N) versus $\langle r_A \rangle$ for six compositions in the $(Ln,Ln')_{0.5}(A,A')_{0.5}MnO_3$ series.

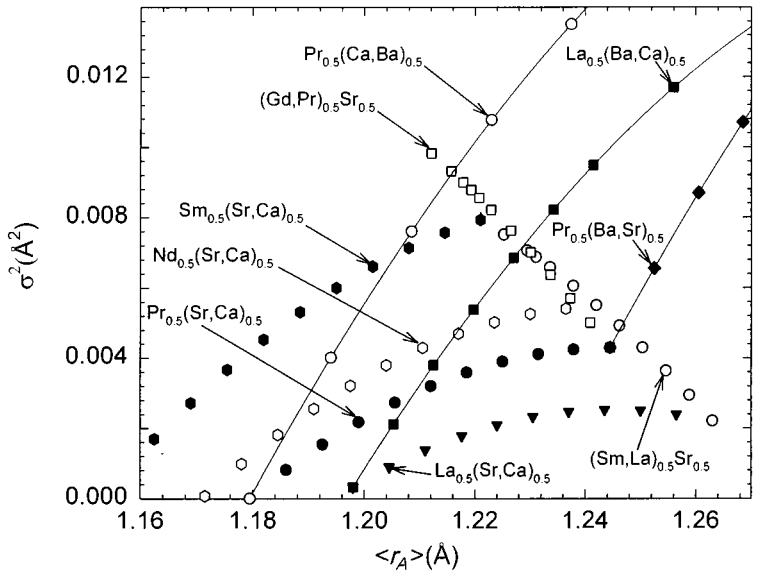

Figure 13. Variance of the A-site cationic radius σ^2 versus average A-site cationic size $\langle r_A \rangle$ for the nine compositions in the series labelled on the graph.

the $\sigma^2(\langle r_A \rangle)$ curves (figure 13). In fact, the A-site mismatch (σ^2) increases and then decreases with $\langle r_A \rangle$ for the $Ln_{0.5}(Sr,Ca)_{0.5}MnO_3$ series whereas it decreases with $\langle r_A \rangle$ for the $(Ln,Ln')_{0.5}Sr_{0.5}MnO_3$ series. One can thus qualitatively explain the results. The Ca for Sr substitution tends to depress T_C due to the decrease of $\langle r_A \rangle$ but this effect is reduced by the fact that simultaneously the mismatch effect decreases,

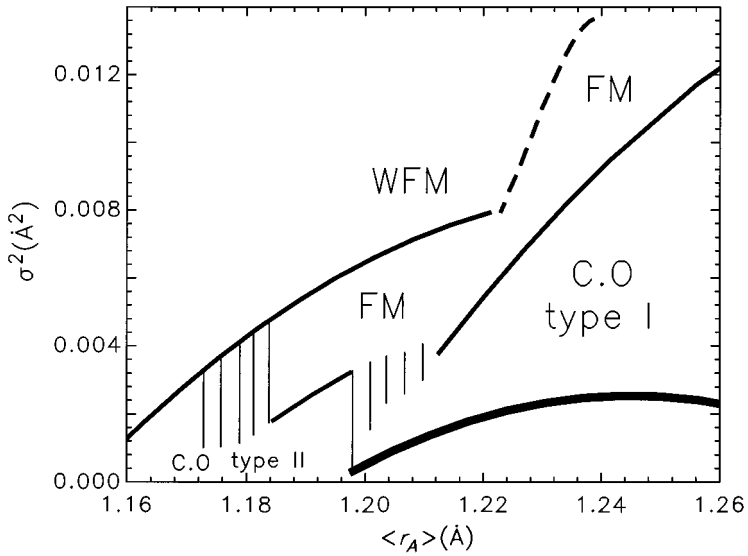

Figure 14. Magnetic phase regions in the $(\sigma^2, \langle r_A \rangle)$ plane for the $Ln_{0.5}A_{0.5}MnO_3$ compounds. Intermediate state areas are dashed.

favouring not only the FMM state but also the AFMI state if one refers to the T_N maxima of nearly 200 K. On the other hand, for the $(Ln_{0.5-y}Ln'_y)Sr_{0.5}MnO_3$ series, σ^2 increases and $\langle r_A \rangle$ decreases simultaneously as y increases so that both effects are cumulative on T_C. $T_C(\langle r_A \rangle)$ and $T_N(\langle r_A \rangle)$ curves collapse in a unique $T_C(\langle r_A \rangle)$ curve below 1.23 Å (figure 12) and thus for the region corresponding to $\langle r_A \rangle < 1.23$ Å the AFMI state is suppressed. Consequently, the observed T_N values for these series are limited to 150 K.

Now, by considering for each sample its σ^2 and $\langle r_A \rangle$ values, a new magnetic diagram is established (figure 14). It shows that samples involving high mismatch effects exhibit a weak ferromagnetic behaviour (WFM on figure 14). This means that even in large magnetic fields (*ca.* 1.4 T) the saturation magnetization remains much smaller than the $3.5\mu_B$ expected value. However, the mismatch effect becomes less efficient as $\langle r_A \rangle$ increases. The thickest solid line of figure 14 is a limit below which no $(Ln,Ln')_{0.5}(A,A')_{0.5}MnO_3$ phase exists. The most interesting information from this diagram is the existence of two different regions where the samples exhibit a CL state. The former, called type I, corresponds to samples characterized by two transitions AFMI–FMM–PMI, whereas the type II compounds (low σ^2 and $\langle r_A \rangle$ values) show only one AFMI–PMI transition.

Finally, this diagram allows the magnetotransport properties of a $Ln_{0.5}A_{0.5}MnO_3$ sample to be predicted by considering its $\langle r_A \rangle$ and σ^2 values. For instance, the $Pr_{0.5}Sr_{0.5}MnO_3$ manganite ($\langle r_A \rangle = 1.2445$ Å and $\sigma^2 = 4.2 \times 10^{-3}$ Å^2) is a type I CL manganite. $Sm_{0.42}Pr_{0.08}Sr_{0.5}MnO_3$ ($\langle r_A \rangle = 1.225$ Å and $\sigma^2 = 7.4 \times 10^{-3}$ Å^2) is an FM compound exhibiting solely an FMM–PMI transition (CD). For the compound $Pr_{0.5}Ca_{0.5}MnO_3$, since

$$r_{Pr^{3+}_{IX}} \sim r_{Ca^{2+}_{IX}} \sim 1.18 \text{ Å}$$

(Shannon 1976), the σ^2 value is the smallest value ($\sigma^2 = 2 \times 10^{-7}$ Å^2) among all the

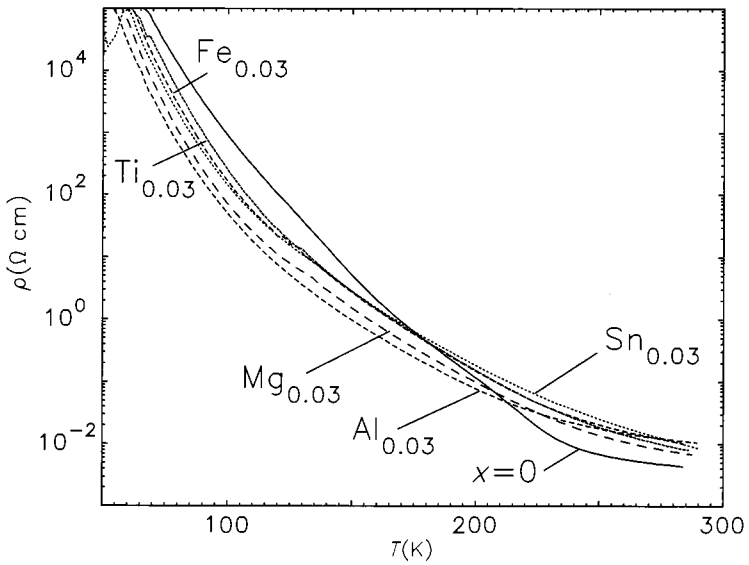

Figure 15. $R(T)$ curves of $Pr_{0.5}Ca_{0.5}MnO_3$ (pristine compound) and of the corresponding doped manganites $Pr_{0.5}Ca_{0.5}Mn_{0.97}M_{0.03}O_3$ ($M = Mg^{2+}$, Al^{2+}, Fe^{3+}, Ti^{4+}, Sn^{4+}).

$Ln_{0.5}A_{0.5}MnO_3$ manganites. This favours the charge-ordering type II. It is also interesting to note that the whole $Pr_{1-x}Ca_xMnO_3$ series is practically 'zero-mismatched'.

(*b*) Mn-*site doping in the* $Pr_{0.5}Ca_{0.5}MnO_3$ *CO compounds* ($M = Mg^{2+}$, Fe^{3+}, Al^{3+}, Ga^{3+}, Ti^{4+}, Sn^{4+})

The CE-type AFM CO magnetic structure of this manganite was first reported by Jirak *et al*. (1985). As mentioned previously, the joint low σ^2 and $\langle r_A \rangle$ values strongly favour Mn^{3+} and Mn^{4+} ordering (i.e. type II). The signature of this ordering on the resistivity curve is a slight change of slope at $T_{CO} = 250$ K (figure 15, curve $x = 0$). This transition temperature is in good agreement with the orbital ordering temperature of the Mn^{3+} and Mn^{4+} species, which involves a doubling of one cell parameter below T_{CO} as evidenced from the powder neutron diffraction studies (Jirak *et al*. 1985). At T_{CO} there exists also a drop in magnetic susceptibility as shown on the $\chi'(T)$ curve (figure 16, curve $x = 0$), χ' values decreasing below $T_{CO} = 250$ K. The high stability of the CO structure is demonstrated in figure 17 where even a magnetic field of 7 T is not sufficient to induce magnetoresistance.

In contrast, by doping the Mn-site with divalent, trivalent or tetravalent cations such as $M = Mg^{2+}$, Fe^{3+}, Al^{3+}, Ti^{4+}, Sn^{4+} the signatures of the CO on both $\rho(T)$ (figure 15) and $\chi'(T)$ (figure 16) curves disappear with only 3% of dopant (Damay 1998). Clearly, the presence of such elements hinders the Mn^{3+} and Mn^{4+} ordering at T_{CO}. Accordingly, a weak ferromagnetic component is induced at low T on the $\chi'(T)$ curves (figure 16). CMR properties are consequently induced by doping as shown in figure 17 for $Pr_{0.5}Ca_{0.5}Mn_{0.97}Fe_{0.03}O_3$.

A similar effect was previously reported in the case of the Fe_3O_4 and Ti_4O_7 compounds for which doping levels of only 1% were found to suppress their Verwey transitions (Mott 1974). This 'impurity effect' on the CO phenomenon is not limited to the three-dimensional CO perovskites but has also been observed for the

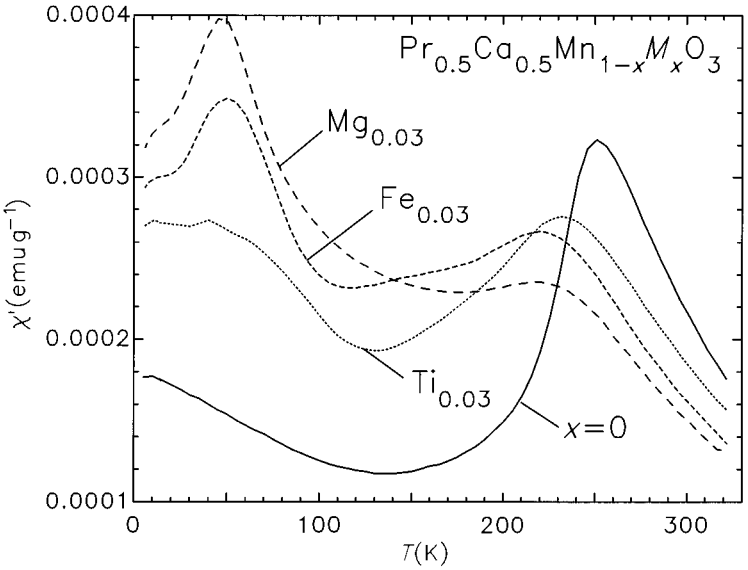

Figure 16. T dependence of the real part of the susceptibility (χ') for $Pr_{0.5}Ca_{0.5}MnO_3$ and 3% doped $Pr_{0.5}Ca_{0.5}Mn_{0.97}M_{0.03}O_3$ samples ($M = Mg^{2+}$, Fe^{3+}, Ti^{4+}).

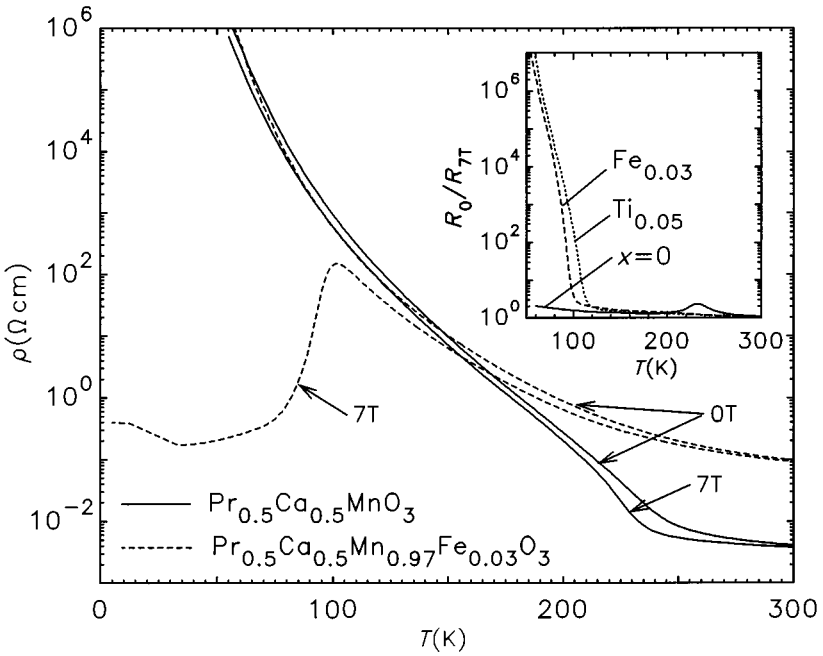

Figure 17. Dependence of the resistivity (ρ) on T for $Pr_{0.5}Ca_{0.5}MnO_3$ and $Pr_{0.5}Ca_{0.5}Mn_{0.97}Fe_{0.03}O_3$ registered in 0 and 7 T. Inset: dependence on T of the $R_0/R_{7\,T}$ ratios demonstrating the CMR induced by doping with M = Fe and Ti.

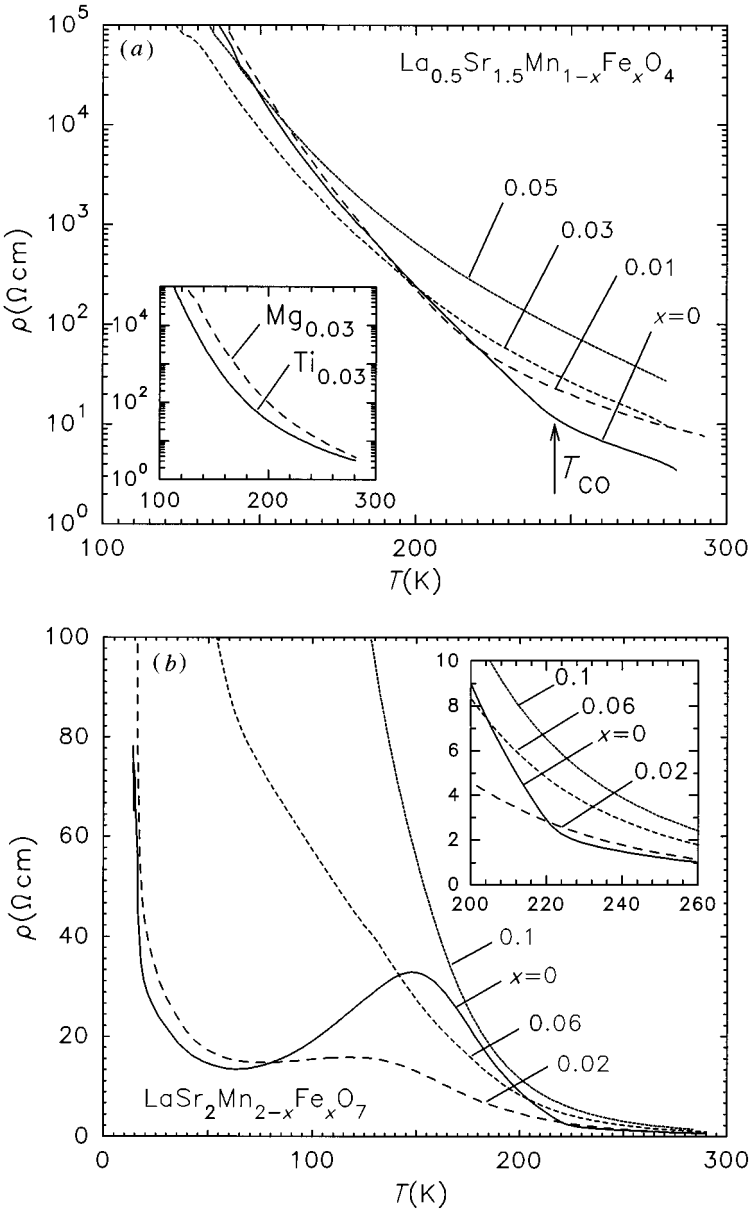

Figure 18. $\rho(T)$ curves for the $La_{0.5}Sr_{1.5}Mn_{1-x}Fe_xO_4$ series (a) and $LaSr_2Mn_{2-x}Fe_xO_7$ series (b). In the insets, the enlargements show the lack of change of slope at T_{CO} for the doped manganites.

CO layered manganites $La_{0.5}Sr_{1.5}MnO_4$ and $LaSr_2Mn_2O_7$ corresponding to the first ($m = 1$) and second members ($m = 2$) of the $(SrO)(La_{1-x}Sr_xMnO_3)_m$ series (Damay *et al*. 1998). For both two-dimensional manganites, the La/Sr ratio has been chosen in order to keep the Mn^{4+}/Mn^{3+} ratio equal to one. Their $\rho(T)_{H=0}$ curves exhibit the characteristic anomaly at $T_{CO} = 220$–240 K (figure 18). However, one can remark on the $m = 2$ curve (figure 18*b*) that there remains some ferromagnetic contribution

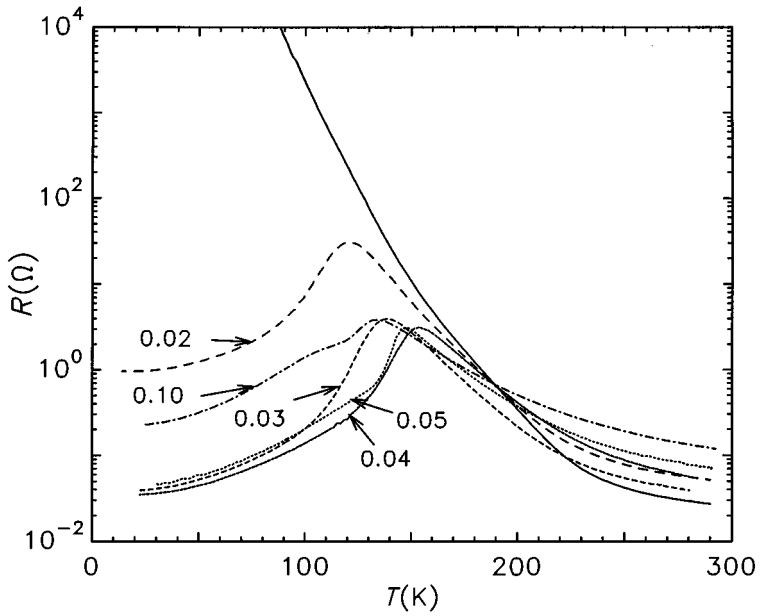

Figure 19. $R(T)$ curves of the $Pr_{0.5}Ca_{0.5}Mn_{1-x}Cr_xO_3$ samples. Solid line corresponds to $x = 0$.

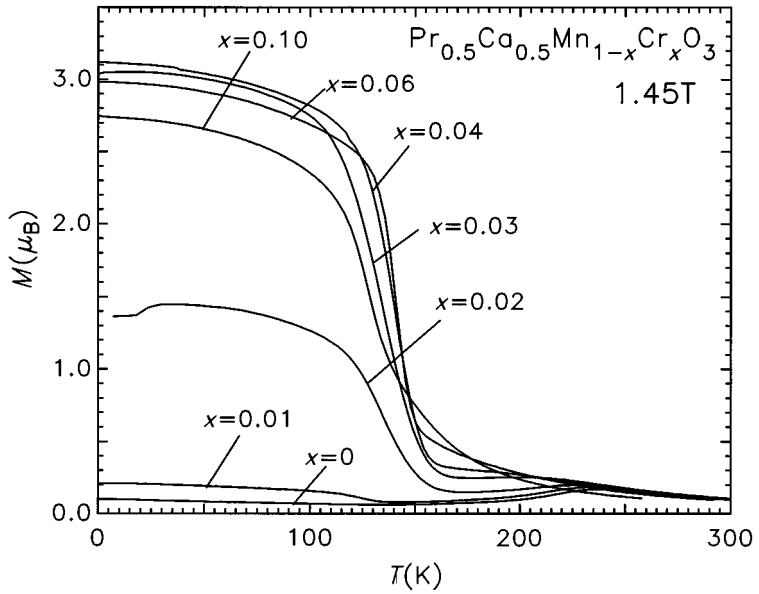

Figure 20. $Pr_{0.5}Ca_{0.5}Mn_{1-x}Cr_xO_3$: $M(T)$ curves.

that may explain the MI transition observed at *ca.* 150 K. Nevertheless, for both manganites, 1% of iron is sufficient to suppress the bump associated with the CO. The similarity of the results obtained for the two- and three-dimensional CO manganites demonstrates that a very small amount of disorder on the Mn lattice is sufficient to strongly modify the magnetotransport properties. Furthermore, in the case of the perovskite, these Mn-site substitutions induce CMR properties.

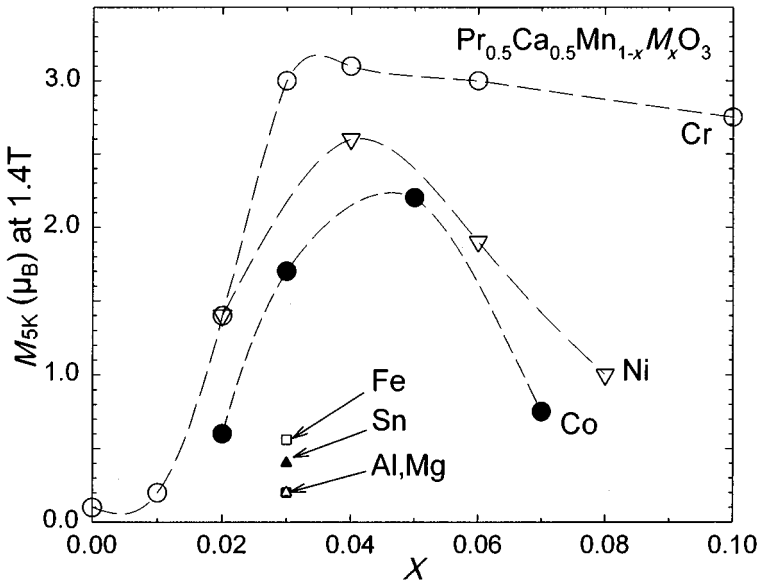

Figure 21. $M_{5\,\mathrm{K}}$ versus x in the $Pr_{0.5}Ca_{0.5}Mn_{1-x}M_xO_3$ series with M = Cr, Ni, Co and, for $x = 0.03$, with M = Mg, Al, Fe, Sn.

(*c*) 'Cr, Co, Ni' *doped* $Ln_{0.5}Ca_{0.5}MnO_3$ *manganites*

In the $Pr_{0.5}Ca_{0.5}Mn_{1-x}M_xO_3$ series (Raveau *et al*. 1997; Maignan *et al*. 1997*b*; Barnabé *et al*. 1997), the most spectacular effect is obtained for M = Cr, Co and Ni. A magnetic field is not required to induce MI transitions in these compounds. Clear transitions are observed on the $R(T)_{H=0}$ curves of the $Pr_{0.5}Ca_{0.5}Mn_{1-x}Cr_xO_3$ samples at values of x as low as $x = 0.02$ (figure 19). The metallic character observed below T_m is associated with the induced ferromagnetism (figure 20). Large saturation magnetization values, up to $3\mu_B$ mol^{-1} of Mn, are restored, in contrast to the small value obtained for the pure sample (*ca.* $0.1\mu_B$). Chromium is in fact the most efficient cation to induce ferromagnetism. The comparison of the saturation magnetization registered at 5 K ($M_{5\,\mathrm{K}}$) for different $Pr_{0.5}Ca_{0.5}Mn_{1-x}M_xO_3$ series demonstrates the superiority of Cr over Ni and Co for which $M_{5\,\mathrm{K}}$ remain lower than $3\mu_B$ (figure 21). Moreover, the effect of Cr remains up to $x = 0.10$, whereas the parabolic curves $M_{5\,\mathrm{K}}(x)$ obtained for M = Co and Ni show that, as soon as $x = 0.05$, $M_{5\,\mathrm{K}}$ begins to decrease. Note also the smaller $M_{5\,\mathrm{K}}$ values obtained for M = Fe^{3+}, Sn^{4+}, Al^{3+} and Mg^{2+} in comparison with those reached for M = Co, Ni and Cr.

The consequence of Cr doping on the CMR is to restore a behaviour characteristic of CD manganites. This is illustrated on figure 22, where the $\rho(T)$ curves registered in 0 and 7 T for $Pr_{0.5}Ca_{0.5}Mn_{0.97}Cr_{0.03}O_3$ and $Pr_{0.7}Ca_{0.2}Sr_{0.1}MnO_3$ are given.

In a general way, the Mn-site doping effect cannot be explained by considering the variation of the Mn^{3+}/Mn^{4+} ratio induced by the foreign cation since all the undoped $Pr_{1-x}Ca_xMnO_3$ series exhibit an insulating behaviour. The different behaviour of M = Co, Cr and Ni compared to M = Mg^{2+}, Fe^{3+}, Al^{3+}, Ga^{3+}, In^{3+}, Sn^{4+}, Ti^{4+} suggests that, although all these dopants destroy CO, something more is required to induce ferromagnetism and the metallicity observed in the 'Cr-, Co-, Ni-' doped phases. For instance, Cr decreases the critical size $\langle r_A \rangle_C$ below which no more MI

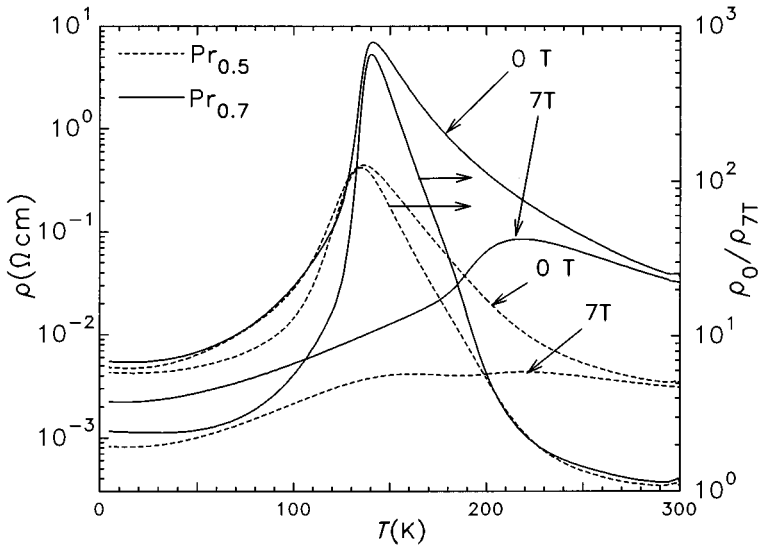

Figure 22. $\rho(T)$ registered in 0 and 7 T and the corresponding ratio $\rho_0(T)/\rho_{7\,\mathrm{T}}(T)$ for the Cr-doped $Pr_{0.5}Ca_{0.5}Mn_{0.97}Cr_{0.03}O_3$ manganite. The same curves for a 'classical' CD $Ln_{0.7}A_{0.3}MnO_3$ manganite are also given.

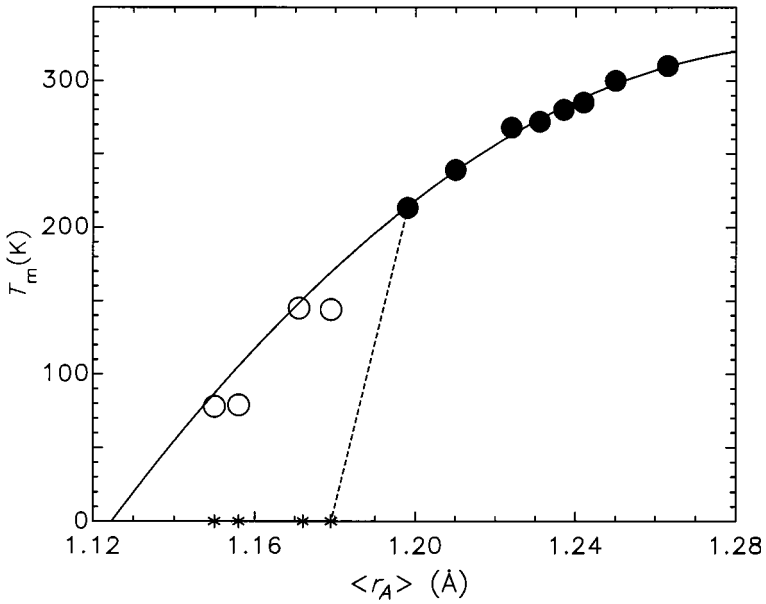

Figure 23. T_m versus $\langle r_\mathrm{A}\rangle$ obtained for different pure $Ln_{0.5}Ca_{0.5}MnO_3$ samples (•); the stars (∗) correspond to the AFMI compositions. (○) are for the corresponding optimally Cr-doped compounds. The MI transition suppression occurring below $\langle r_\mathrm{A}\rangle \sim 1.19$ Å for the pure samples is restored by Cr doping for 1.14 Å $< \langle r_\mathrm{A}\rangle <$ 1.19 Å.

transition is observed. For the pure $Ln_{0.5}Ca_{0.5}MnO_3$ compounds, this limit is $\langle r_\mathrm{A}\rangle_\mathrm{C} =$ 1.19 Å as shown in figure 23. By optimally doping these perovskites with Cr, MI transitions are thus induced down to $\langle r_\mathrm{A}\rangle_{\mathrm{C}'} = 1.14$ Å.

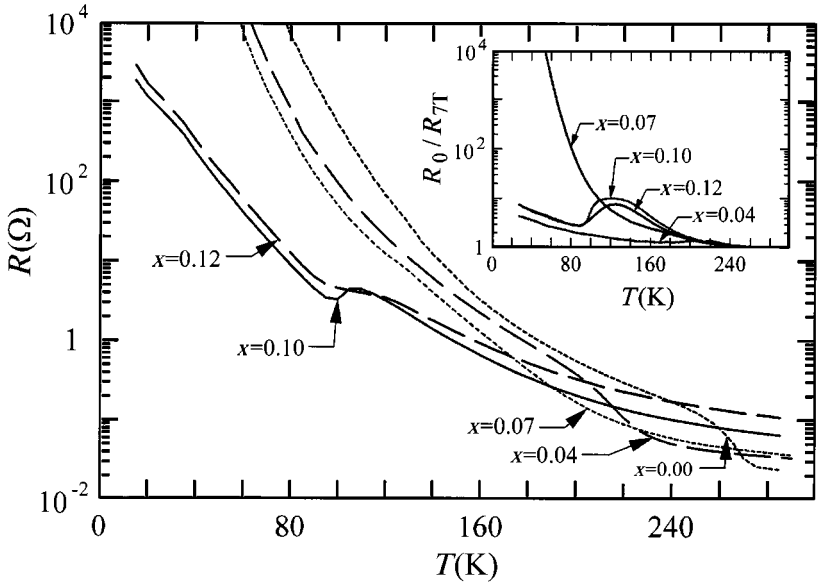

Figure 24. $R(T)$ curves for the $Pr_{0.4}Ca_{0.6}Mn_{1-x}Cr_xO_3$ samples registered in zero magnetic field. Inset, $R_0/R_{7\,T}$ curves.

(*d*) *Role of the carrier density:* $Pr_{1-y}Ca_yMn_{1-x}Cr_xO_3$

In order to understand the role of the carrier density we have carried out a study of Cr-doped $Pr_{1-y}Ca_yMnO_3$ samples. For the Mn^{4+}/Mn^{3+} ratios larger than unity (Barnabé *et al.* 1998), a re-entrant transition is hardly visible on the $R(T)$ curves, as illustrated for $Pr_{0.4}Ca_{0.6}Mn_{1-x}Cr_xO_3$ samples with $x = 0.10$ and 0.12 (figure 24). For smaller x values, the CO characteristic change of slope still exists although T_{CO} decreases from 270 K for $x = 0.0$ to 240 K for $x = 0.07$ (figure 24). It seems likely that for this series at 60% of Mn^{4+}, the charge-ordering is more difficult to weaken so that larger Cr contents are required to induce solely a re-entrant resistive transition. Nevertheless, CMR effects are still induced by application of a magnetic field for these Cr-doped samples with $0.12 \geqslant x \geqslant 0.07$ (inset of figure 24). For an even higher Mn^{4+} content the Cr efficiency is further decreased so that for the $Pr_{0.3}Ca_{0.7}Mn_{1-x}Cr_xO_3$ series, no more transition is induced on the $R(T)_{H=0}$ curves.

For Mn^{4+}/Mn^{3+} ratios smaller than one ($0.33 \leqslant y < 0.5$) the Cr for Mn substitution remains an efficient way to induce MI transitions. $R(T)$ curves are reported for four series corresponding to $y = 0.40$, 0.35, 0.34 and 0.30 in $Pr_{1-y}Ca_yMn_{1-x}Cr_xO_3$ (figure 25). From the observation of these sets of $R(T)$ curves, it appears that the amount of Cr required to induce the MI transition increases with decreasing Mn^{4+} content. For $Pr_{0.6}Ca_{0.4}MnO_3$ ($y = 0.40$) only 0.5% of Cr is needed to induce a transition at $T_m = 60$ K (figure 25*a*), whereas 2% and 4% are necessary for $Pr_{0.65}Ca_{0.35}MnO_3$ and $Pr_{0.66}Ca_{0.34}MnO_3$, respectively (figure 25*b*, *c*); finally, a MI transition could not be induced in $Pr_{0.7}Ca_{0.3}MnO_3$ whatever the Cr content up to 8% (figure 25*d*).

A more detailed analysis of the $R(T)$ curves allows the following comments to be made.

(i) For the $Pr_{0.6}Ca_{0.4}Mn_{1-x}Cr_xMnO_3$ series, one can notice the existence, for $x =$

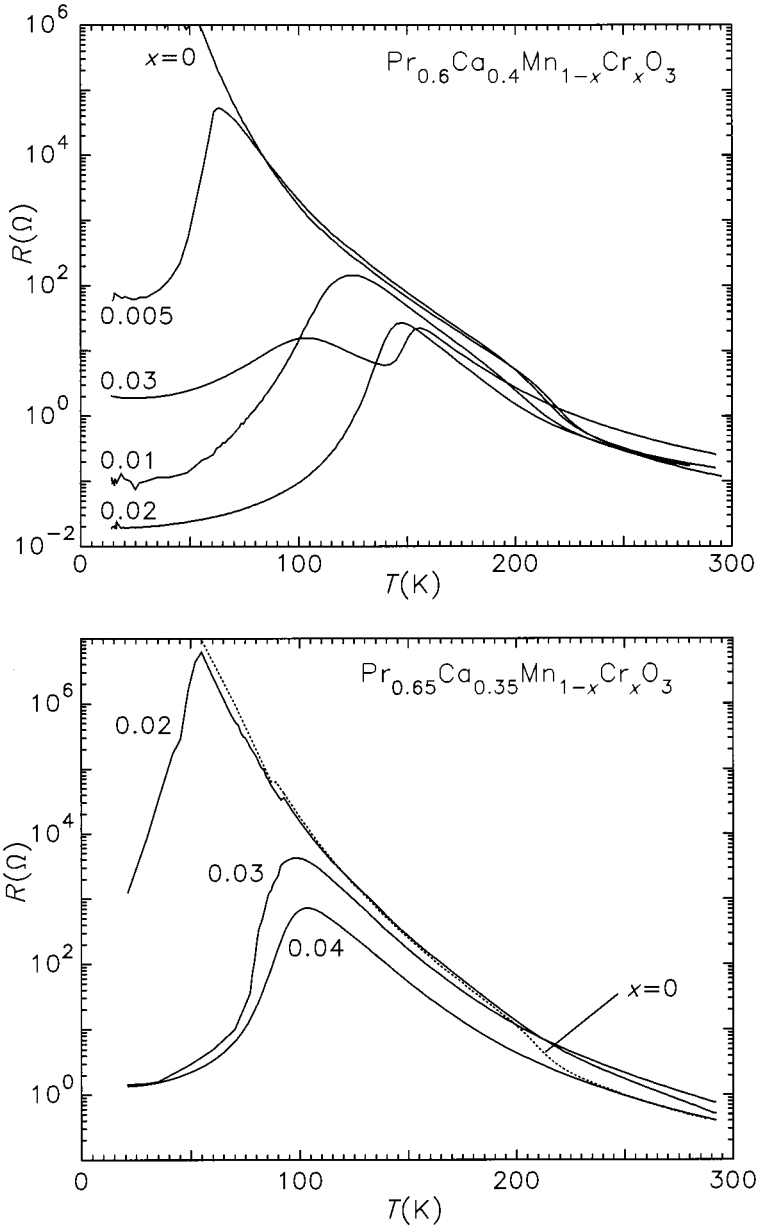

Figure 25. $R(T)$ curves of four Cr-doped compositions in the $Pr_{1-y}Ca_yMnO_3$ series: (top) $y = 0.4$; (bottom) $y = 0.65$.

0.005 and $x = 0.01$, of both the induced MI transition and the bump at T_{CO}. These features are confirmed by the $M(T)$ curves (figure 26) showing the FM transitions and also small bumps at about 200 K related to the AFM transitions. This behaviour, not observed for $y = 0.5$ (figure 19) and $y = 0.35$ (figure 25*b*), may result from the CE-type canted magnetic structure of $Pr_{0.6}Ca_{0.4}MnO_3$ (Jirak *et al.* 1985) for which the Cr effect may act differently.

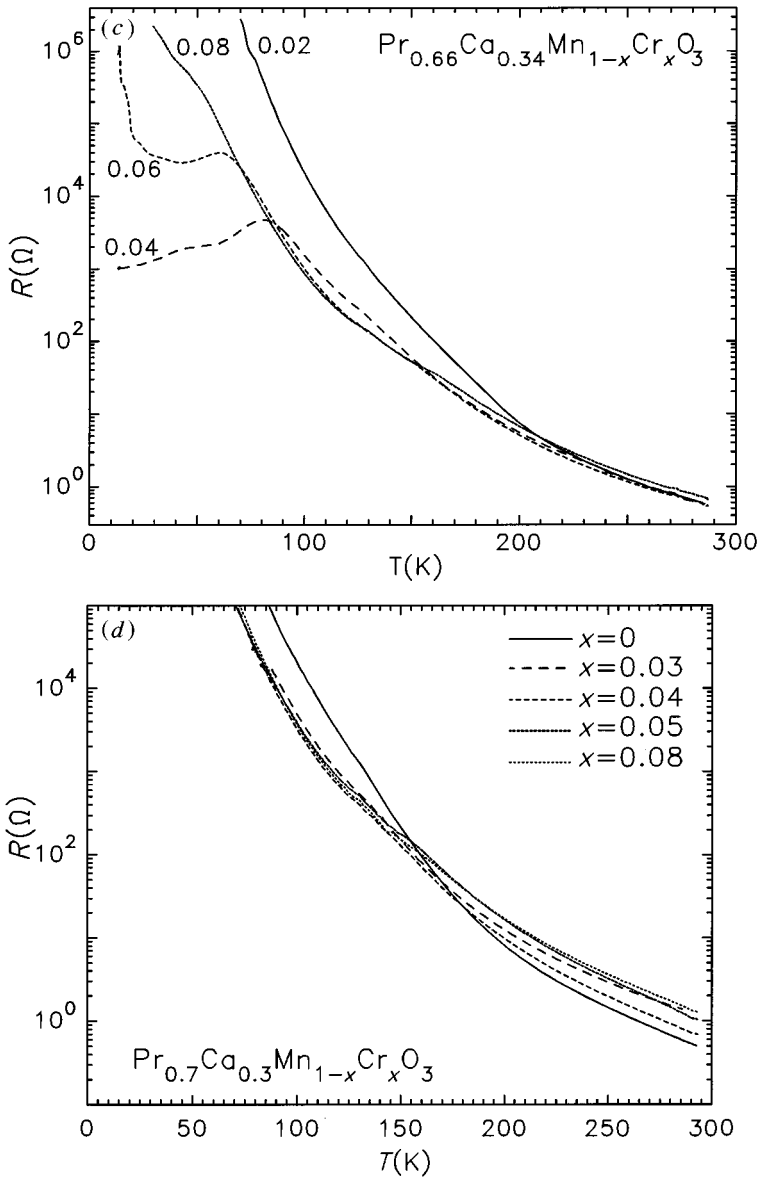

Figure 25. (*Cont.*) (top) $y = 0.34$; (bottom) $y = 0.30$.

(ii) For the $Pr_{0.66}Ca_{0.34}MnO_3$ series, the MI transition is less unequivocal than for other doped manganites since the resistance values below T_M remain high (figure 25*c*). This indicates that the '$Pr_{0.66}Ca_{0.34}$' composition represents the limit toward the low Mn^{4+} content of the Cr effect. The results obtained for $y = 0.3$, for which the samples remain insulating whatever the Cr content (figure 25*d*), corroborate this assumption. This result is quite unexpected if one refers to the magnetic structure of $Pr_{0.7}Ca_{0.3}MnO_3$ (Jirak *et al.* 1985) which exhibits a ferromagnetic component. Moreover, the $M(T)$ curves show that the ferromagnetic state is well reinforced by the Cr substitution (figure 27). Starting from $2.6\mu_B$ for $x = 0$, M reaches

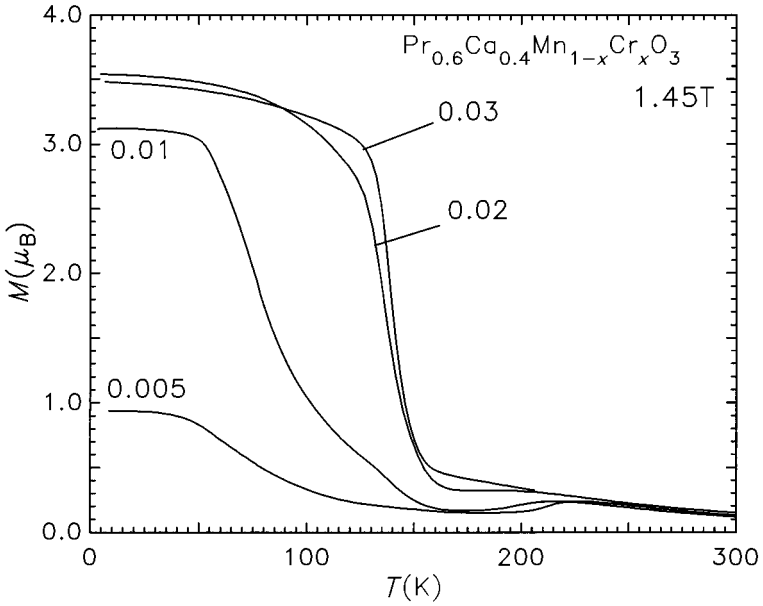

Figure 26. $M(T)$ curves of the $Pr_{0.6}Ca_{0.4}Mn_{1-x}Cr_xO_3$ samples.

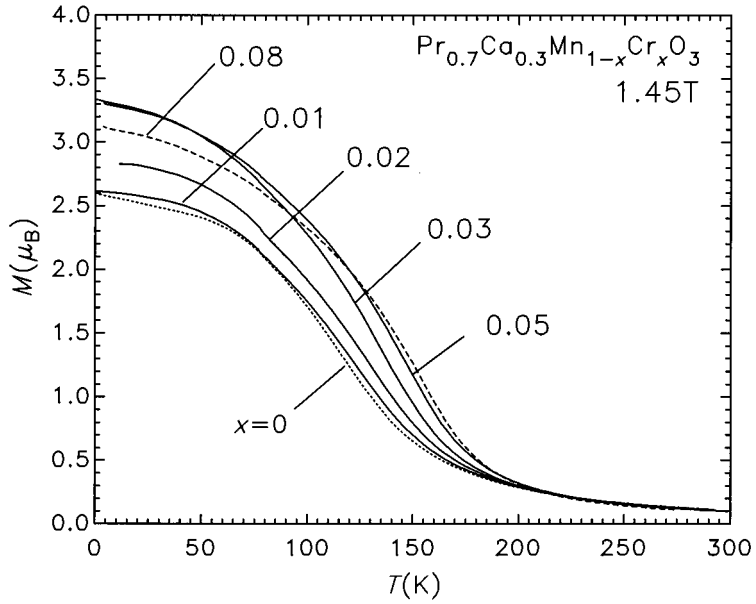

Figure 27. $M(T)$ curves of the $Pr_{0.7}Ca_{0.3}Mn_{1-x}Cr_xO_3$ series.

$3.3\mu_B$ mol^{-1} of Mn for $x = 0.03$. Moreover, T_C increases simultaneously with M. The magnetization measurements thus indicate a ferromagnetic behaviour in spite of the lack of MI transition on the $R(T)$ curves.

In conclusion, the Cr-induced MI transition exists on both sides of the $Pr_{0.5}Ca_{0.5}MnO_3$ composition, for $0.3 < y < 0.7$. This result emphasizes that Cr doping induces

a MI transition provided the undoped sample be CO and, *a contrario*, for a strongly ferromagnetic undoped sample, the Cr efficiency decreases significantly.

4. Conclusion

This study shows the great influence of Mn-site doping on the properties of manganites. For the CD compounds such as $Sm_{0.56}Sr_{0.44}Mn_{1-x}M_xO_3$, a few per cent of dopant is sufficient to dramatically weaken T_C. However, the effect on T_C depends on the doping element, decreasing from $dT_C/dx = -25\,K\,\%^{-1}$ for $M = Fe^{3+}$ and Sn^{4+} to $dT_C/dx = -10$ to $-12\,K\,\%^{-1}$ for Ni and Co. Interestingly, Cr-doped samples exhibit a different behaviour since no effect on T_C is observed, at least up to 5% of Cr. The regular decrease of T_C demonstrated for different cations such as $M = Mg^{2+}$, Fe^{3+}, Al^{3+}, Ga^{3+}, Sn^{4+} and Ti^{4+} allows T_C of these manganites to be tuned so that huge CMR effects can be induced.

Among the $Ln_{0.5}A_{0.5}MnO_3$ manganites, the compounds characterized by a small size of the A-site cation and a low-cation-size mismatch are of particular interest for the Mn-site doping effect. In these CO manganites, Mn-site doping tends to weaken the AFM interactions, thereby restoring some ferromagnetic contribution. The substituted elements thus play the role of impurities that hinder the CO establishment. This effect is also observed for two-dimensional manganites such as $La_{0.5}Sr_{1.5}MnO_4$ and $LaSr_2Mn_2O_7$ compounds. Such substitutions in the CO perovskites are an efficient means of inducing CMR. For M = Cr, Co and Ni the effect is even more spectacular since a MI transition is induced, as shown for $Pr_{0.5}Ca_{0.5}MnO_3$. In particular, for Cr, the critical $\langle r_A \rangle$ size below which no more MI transition is observed can be pushed down. Moreover, the MI transition associated with the ferromagnetism induced by Cr is observed for $Pr_{1-y}Ca_yMnO_3$ with $0.3 < y < 0.7$ showing that the effect is not limited to the commensurate $Mn^{3+}/Mn^{4+} = 1$ ratio. Finally, it must be emphasized that the similar electronic configuration of Cr^{3+} and Mn^{4+} may be at the origin of the different role played by Cr. The present results suggest that this element participates in the double-exchange mechanism.

References

Barnabé, A., Maignan, A., Hervieu, M., Damay, F., Martin, C. & Raveau, B. 1997 *Appl. Phys. Lett.* **71**, 3907.

Barnabé, A., Maignan, A., Hervieu, M. & Raveau, B. 1998 *Eur. Phys. J.* B **1**, 145.

Chahara, K., Ohno, T., Kasai, M. & Kozono, Y. 1993 *Appl. Phys. Lett.* **63**, 1990.

Damay, F., Nguyen, N., Maignan, A., Hervieu, M. & Raveau, B. 1996*a* *Solid State Commun.* **98**, 97.

Damay, F., Maignan, A., Nguyen, N. & Raveau, B. 1996*b* *J. Solid State Chem.* **124**, 385.

Damay, F., Martin, C., Maignan, A. & Raveau, B. 1997*a* *J. Appl. Phys.* **81**, 1372.

Damay, F., Martin, C., Maignan, A. & Raveau, B. 1997*b* *J. Appl. Phys.* **82**, 6181.

Damay, F., Martin, C., Maignan, A. & Raveau, B. 1998 *J. Magn. Magn. Mater* **183**, 143.

Jin, S., Tiefel, T. H., McCormack, M., Fastnacht, R. A., Mahesh, R. & Chen, L. H. 1994 *Science* **264**, 413.

Jirak, Z., Krupicka, S., Nekvasil, V., Pollert, E., Villeneuve, G. & Zounova, F. 1980 *J. Magn. Magn. Mater.* **15**, 519.

Jirak, Z., Krupicka, S., Simsa, Z., Dlouha, M. & Vratislav, S. 1985 *J. Magn. Magn. Mater.* **53**, 153.

Jonker, G. H. 1956 *Physica* **22**, 707.
Ju, H. L., Kwon, C., Li, Qi, Greene, R. L. & Venkatesan, T. 1994 *Appl. Phys. Lett.* **65**, 2108.
Kawano, H., Kajimoto, R., Yoshizawa, H., Tomioka, Y., Kuwahara, H. & Tokura, Y. 1997 *Phys. Rev. Lett.* **78**, 4253.
Kuwahara, H., Tomioka, Y., Asamitsu, A., Moritomo, Y. & Tokura, Y. 1995 *Science* **270**, 961.
Mahendiran, R., Mahesh, R., Raychaudhuri, A. K. & Rao, C. N. R. 1995 *Solid State Commun.* **94**, 515.
Mahesh, R., Mahendiran, R., Raychaudhuri, A. K. & Rao, C. N. R. 1995*a* *J. Solid State Chem.* **114**, 297.
Mahesh, R., Mahendiran, R., Raychaudhuri, A. K. & Rao, C. N. R. 1995*b* *J. Solid State Chem.* **120**, 204.
Maignan, A., Caignaert, V., Simon, Ch., Hervieu, M. & Raveau, B. 1995*a* *J. Mater. Chem.* **5**, 1089.
Maignan, A., Simon, Ch., Caignaert, V. & Raveau, B. 1995*b* *Solid State Commun.* **96**, 623.
Maignan, A., Simon, Ch., Caignaert, V. & Raveau, B. 1996 *Z. Phys.* B **99**, 305.
Maignan, A. & Raveau, B. 1997 *Z. Phys.* B **102**, 209.
Maignan, A., Martin, C. & Raveau, B. 1997*a* *Z. Phys.* B **102**, 19.
Maignan, A., Damay, F., Martin, C. & Raveau, B. 1997*b* *Mat. Res. Bull.* **32**, 965.
Manoharan, S. S., Vasanthacharya, N. Y., Hedge, M. S., Satyalakshmi, K. M., Prasad, V. & Subramanyam, S. V. 1994 *J. Appl. Phys.* **76**, 3923.
Martin, C., Maignan, A. & Raveau, B. 1996 *J. Mater. Chem.* **6**, 1245.
Mott, N. F. 1974 *Metal–insulator transitions*, 2nd edn. London: Taylor & Francis.
Pollert, E., Krupicka, S., Simsa, Z., Dlouha, M. & Vratislav, S. 1982 *J. Phys. Chem. Solids* **43**, 1137.
Raveau, B., Maignan, A. & Martin, C. 1997 *J. Solid State Chem.* **130**, 162.
Rodriguez-Martinez, L. M. & Attfield, J. P. 1996 *Phys. Rev.* B **54**, R15 622.
Shannon, R. D. 1976 *Acta Crystallogr.* A **32**, 751.
Tomioka, Y., Asamitsu, A., Moritomo, Y., Kuwahara, H. & Tokura, Y. 1995 *Phys. Rev. Lett.* **74**, 5108.
Von Helmolt, R., Wecker, J., Holzapfel, B., Schultz, L. & Samwer, K. 1993 *Phys. Rev. Lett.* **71**, 2331.
Wang, H. Y., Cheong, S. W., Radaelli, P. G., Marezio, M. & Batlogg, B. 1995 *Phys. Rev. Lett.* **75**, 914.
Wolfman, J., Simon, Ch., Hervieu, M., Maignan, A. & Raveau, B. 1996*a* *J. Solid State Chem.* **123**, 413.
Wolfman, J., Maignan, A., Simon, Ch. & Raveau, B. 1996*b* *J. Magn. Magn. Mater.* **159**, L299.
Wollan, E. O. & Koehler, W. C. 1955 *Phys. Rev.* **100**, 545.

Discussion

P. Battle (*University of Oxford, UK*). When he puts Ni and the like in, is Dr Maignan confident that it remains O_3, that the oxygen sublattice is full?

A. Maignan. We currently have no neutron information that the oxygen stoichiometry is less than 3.

P. Battle. So, when he puts Ni and Co in, what oxidation state should I think of them as being in?

A. Maignan. The Mn^{3+} content is decreased, but normally these materials are insulating from 0.25 to 0.5, so if the valency is changed by 2%, the behaviour is completely changed. Thus I think this is not a good explanation of the difference.

J. P. Attfield (*University of Cambridge, UK*). For the samples which show both a Néel temperature and a Curie temperature, has Dr Maignan looked at diffraction or other methods to see whether the structural distortions occur at those two transitions?

A. Maignan. Yes, but I think there are two types of transition that occur in this material, one at the Néel temperature and one at high temperatures.

J. P. Attfield. Does the magnitude of the structural change at T_C or T_N correlate in any way with their sensitivity to either A cation size or disorder?

A. Maignan. We have no structural evidence at the moment as to what happens when we just put in disorder. A good probe is NMR because it is a local method and when you turn to the substituted sample you get a very different spectrum from samples which are insulators. At an atomic scale, you restore the classical spectrum of a sharply localized material, so that an atomic scale is no problem; it is like an LaSr compound.

A. J. Millis (*The Johns Hopkins University, USA*). Dr Maignan showed a series of resistivity curves (figures 16 and 17) which showed that when he substituted on the B-site, the resistivity rose very rapidly, and yet was apparently temperature independent at low temperatures. Why is the resistivity so extremely sensitive to the B-site substitution?

A. Maignan. I think it is due to the scattering of the carriers on the B-site.

A. J. Millis. But increasing the resistivity by orders of magnitude? It cannot just be scattering from a few per cent of defects. That is what confused me. So in figure 17, there is just 3% doping on the B-site, and yet the resistivity changed by a factor of 100. Why?

A. Maignan. The Curie temperature is decreased. All the curves are the same.

A. J. Millis. Why is the residual resistivity at low temperatures changing so much? Why is it so high, and yet so metallic and yet has no temperature dependence?

A. Maignan. I do not know.

T. Venkatesan (*University of Maryland, USA*). We can say that in the charge-ordered case, the Cr doping really helps in getting ferromagnetism, but if I start with something which is already ferromagnetic, what happens?

A. Maignan. If you just put Cr in a ferromagnet, you do not improve the ferromagnetism; and the opposite, if you just go too far in the doping, you destroy the ferromagnetism. So in the PrCa series this is quite spectacular, because the most efficient way to substitute Cr is for $Pr_{0.5}Ca_{0.5}$. If you turn to $Pr_{0.7}Ca_{0.3}$, which is known to get a ferromagnetic component with also antiferromagnetism, you do not switch the sample to metallicity with Cr doping. So the best effect is shown for the most antiferromagnetic sample.

T. T. M. Palstra (*University of Groningen, The Netherlands*). What happens to the charge-ordering temperature if magnetite is Cr-substituted?

A. Maignan. Many years ago, Sir Nevil Mott described the effect of substitution doping in some charge-ordered material, and I think the conclusion is that it destroys the change of slope associated with the charge ordering on the resistivity curve. But he says that there is no clear explanation at the moment, an unknown effect.

PHILOSOPHICAL TRANSACTIONS OF THE ROYAL SOCIETY A MATHEMATICAL, PHYSICAL & ENGINEERING SCIENCES